Oxygen vacancy-mediated room-temperature ferromagnetism in insulating cobalt-substituted $SrTiO_3$ epitaxially integrated with silicon

Agham B. Posadas,[1] Chandrima Mitra,[1] Chungwei Lin,[1] Ajit Dhamdhere,[2] David J. Smith,[2] Maxim Tsoi,[1] and Alexander A. Demkov[1,*]

[1]*Department of Physics, The University of Texas at Austin, Austin, Texas 78712, USA*

[2]*Department of Physics, Arizona State University, Tempe, Arizona 85287, USA*

(Received 23 January 2013; published 29 April 2013)

Room-temperature ferromagnetic insulating behavior is demonstrated in cobalt-substituted $SrTiO_3$ grown on silicon. Ferromagnetism is exhibited by films with a composition of 30–40% cobalt. Measurements of stoichiometry by x-ray photoelectron spectroscopy indicate Co replacing Ti with the concomitant creation of an approximately equal number of oxygen vacancies as the cobalt ions. First-principles modeling of this system shows that the observed local magnetic moment originates from a cobalt-oxygen vacancy complex with Co in the +2 valence state. The calculations also confirm the insulating nature of the material. The ability to deposit a room-temperature ferromagnetic insulator onto silicon may be useful for certain spintronics applications such as spin filters for spin-injection contacts.

DOI: 10.1103/PhysRevB.87.144422 PACS number(s): 71.15.Mb, 75.70.Ak, 77.55.Px, 79.60.Jv

I. INTRODUCTION

The ability to manipulate the spin degrees of freedom in electronic devices, in addition to the traditional control of charge, can potentially lead the way to advanced device structures that have higher speed and lower energy consumption.[1] One such proposed device is the spin-field-effect transistor (spin-FET).[2] The hardest challenge in realizing spin-FETs is the efficient injection of a spin-polarized current from a ferromagnetic metal into a semiconductor such as silicon. Among the issues are the large density of states (DOS) mismatch between a metal and semiconductor, resulting in the injection efficiency of less than 1%,[3] and the fact that the interface between a typical ferromagnetic metal and silicon is chemically unstable, leading to silicide pockets and other defects such as stacking faults.[4] The use of tunnel barriers such as ultrathin MgO or Al_2O_3 layers has partially alleviated the issue, raising injection efficiency to approximately 30%.[5,6] Using dilute magnetic semiconductors as spin-injection contacts is a natural choice, as these materials have high-quality interfaces to regular semiconductors and do not have the conductivity mismatch problem. However, magnetic semiconductors have Curie temperatures well below room temperature (less than 180 K for the best reported magnetic transition temperature), limiting their practical application.[7]

Ever since the report of room-temperature ferromagnetism in doped transition metal oxides by Matsumoto *et al.*,[8] considerable scientific efforts have been driven toward the study of these dilute magnetic oxides due to their potential for various spintronics applications, including spin-injection contacts.[9,10] Several simple metal oxides such as ZnO,[11,12] SnO_2,[13,14] In_2O_3,[15,16] and TiO_2 (Refs. 17 and 18) have been found to exhibit room-temperature ferromagnetism when doped with magnetic ions. There has also been an extensive effort to increase the Curie temperature of these systems as well as to look for new candidates for room-temperature ferromagnetism.[19] One issue limiting the application potential of most ferromagnetic-doped metal oxides is the difficulty of integrating them with a suitable semiconductor spin host such as silicon. Most of the known dilute ferromagnetic oxides are not thermodynamically stable in contact with silicon.[20] For example, ferromagnetic cobalt-doped anatase TiO_2 is known to result in substantial SiO_2 formation and TiO_2 reduction when grown epitaxially on silicon using a $SrTiO_3$ buffer.[21]

$SrTiO_3$ is one of a handful of perovskite oxides that can be epitaxially grown directly on silicon with a clean epitaxial interface,[22] making it a good candidate for the integration of a ferromagnetic oxide onto silicon. A limited amount of work has been reported on using $SrTiO_3$ as a host material for magnetic ion doping with contradictory results. Bulk synthesis methods generally do not show ferromagnetism in cobalt-doped $SrTiO_3$ except when a significant number of oxygen vacancies are present.[23–27] Thin films of insulating/semiconducting cobalt-doped $SrTiO_3$ grown by pulsed-laser deposition (PLD), on the other hand, are reported to exhibit ferromagnetism at very high doping ($>\sim$20%) but not at low doping.[28,29] Cobalt-doped metallic (La,Sr)TiO_3 thin films, however, do show ferromagnetism and highly spin-polarized carriers even at very low doping ($\sim$2%).[30]

In this paper, we demonstrate the epitaxial integration of Co-substituted $SrTiO_3$ on Si by means of a layer sequenced approach using molecular beam epitaxy (MBE). The films exhibit room-temperature insulating ferromagnetic behavior in the composition range of 30–40% cobalt. *In situ* compositional analysis of the films using x-ray photoelectron spectroscopy (XPS) indicates cobalt ions in the +2 valence state substituting for titanium, along with a significant amount of oxygen vacancies. Using first-principles calculations, we also study the magnetic behavior of Co-substituted $SrTiO_3$, with particular emphasis on the role of oxygen vacancies in promoting magnetism. Our results suggest that a cobalt (II) ion-oxygen vacancy complex is responsible for the observed ferromagnetic insulating behavior in this system. Such a room-temperature ferromagnetic insulator that can be integrated on silicon is potentially useful for spin-filtering-type injection contacts in spin-FETs.

II. EXPERIMENTAL

A. Film growth

The cobalt-substituted $SrTiO_3$ samples are grown by MBE on a thin (three-unit cells) undoped $SrTiO_3$ buffer grown on Si(001). Several cobalt-substituted samples were also grown directly on silicon. Growth is performed using a DCA 600 MBE system equipped with effusion cells for Sr and Ti and with an electron beam evaporation source for Co. Molecular oxygen fed through a piezoelectric leak valve is used as the oxidant for this work. Sr and Ti fluxes are calibrated using a combination of flux measurement with a quartz crystal microbalance and the appearance/disappearance of reflection high-energy electron diffraction (RHEED) reconstruction spots when growing undoped $SrTiO_3$. Co flux is measured using the quartz microbalance with feedback from XPS and cobalt metal film thickness measurements. The growth process is monitored *in situ* with RHEED (Staib Instruments) to ensure the film is crystalline and epitaxial. The RHEED measurement is performed using an electron energy of 18 keV and a grazing incidence angle of 4°. Details of the growth process for depositing undoped $SrTiO_3$ on Si are described in Ref. 31.

The cobalt-substituted $SrTiO_3$ is grown at 550 °C on a three-unit cell undoped $SrTiO_3$ on Si substrate under a constant background oxygen partial pressure of 2×10^{-7} torr. The Sr, Co, and Ti fluxes are all adjusted to yield one monolayer per minute. The nominal sample stoichiometry is $SrTi_{1-x}Co_xO_{3-y}$. Samples with target cobalt compositions of $x = 10$, 20, 30, 40, and 50% have been grown. During the growth, the Sr shutter is always open, while the Co and Ti shutters are opened alternately for a length of time corresponding to the target cobalt composition. The films are crystalline and epitaxial as-deposited with no further annealing treatment necessary.

B. Film characterization

After growth, the films are characterized *in situ* using a VG Scienta XPS system with R3000 electron analyzer. High-resolution scans of the Co *2p*, O *1s*, Ti *2p*, and Sr *3d* core levels are performed for each sample to determine stoichiometry. Stoichiometry is calculated using the Physical Electronics atomic sensitivity factors[32] as a basis, corrected using a single-crystal $SrTiO_3$ standard, and accounting for the kinetic energy variation of the electron sampling depth. A monochromated Al $K\alpha$ source ($h\nu = 1486.6$ eV) is used as the excitation source with the x-rays incident at 54.7° from normal. Photoelectrons are collected at normal emission using a pass energy of 100 eV and a slit width of 0.4 mm. The analyzer is calibrated using a two-point measurement of well-known energy levels of Ag (Ag $3d_{5/2}$ at 368.26 eV and Ag Fermi edge at 0.0 eV).

All films are also characterized *ex situ* using x-ray diffraction (Bruker D8 Advance) and magnetometry (Quantum Design MPMS). Magnetization vs magnetic field measurements are performed at 300 and at 10 K in a magnetic field range of ± 10 kOe. Selected samples have been prepared and imaged in cross-sections using a JEOL JEM-4000EX transmission electron microscope operated at 400 keV. Resistivity vs temperature down to liquid nitrogen temperature using a van der Pauw configuration was also measured on a sample exhibiting ferromagnetism to determine whether it is metallic or insulating.

III. COMPUTATIONAL METHODS

To study the electronic structure of Co-substituted $SrTiO_3$, we employ density functional theory (DFT) using the Vienna *Ab initio* Simulation Package code[33] with projector-augmented-wave pseudopotentials.[34] The valence electrons included for Sr, Ti, and Co are $4s^2\ 4p^6\ 5s^2$, $3s^2\ 3p^6\ 4s^2\ 3d^2$, and $4s^2\ 3d^7$, respectively. A plane-wave cutoff energy of 600 eV is used. Calculations are performed on 40- and 135-atom supercells of $SrTiO_3$ in order to model $SrTi_{1-x}Co_xO_{3-\delta}$. Monkhorst-Pack special k-point grids[35] of $4 \times 4 \times 4$ and $6 \times 6 \times 6$ are chosen for the $3 \times 3 \times 3$ and $2 \times 2 \times 2$ supercells, respectively, to integrate over the Brillouin zone. The energies are converged to within 10^{-6} eV/cell. All forces are converged to within 0.004 eV/Å.

In order to take correlation effects of the d electrons of Co into account, we perform local spin density approximation + U calculations employing the simplified, rotationally invariant approach as introduced by Dudarev *et al.*[36] In accordance with results extracted from photoemission data,[37] an effective U, U_{eff}, (where $U_{\text{eff}} = U - J$) of 4.0 eV is added to the Co d states. This value of U_{eff} also results in stabilizing an intermediate spin state of 2.5 μ_B/Co in $SrCoO_3$ which agrees with experimental observations.[38] For the Ti d states, a U_{eff} value of 8.5 eV is added in order to obtain the experimentally observed band gap of 3.2 eV in $SrTiO_3$.[39] We have verified that this high value of U_{eff} on the Ti d states does not affect the magnetic moments of the Co atoms.

IV. RESULTS AND DISCUSSION

A. Film crystalline structure

RHEED patterns for a 10-nm Co-substituted $SrTiO_3$ film grown on 1.5-nm undoped $SrTiO_3$/Si are shown in Fig. 1.

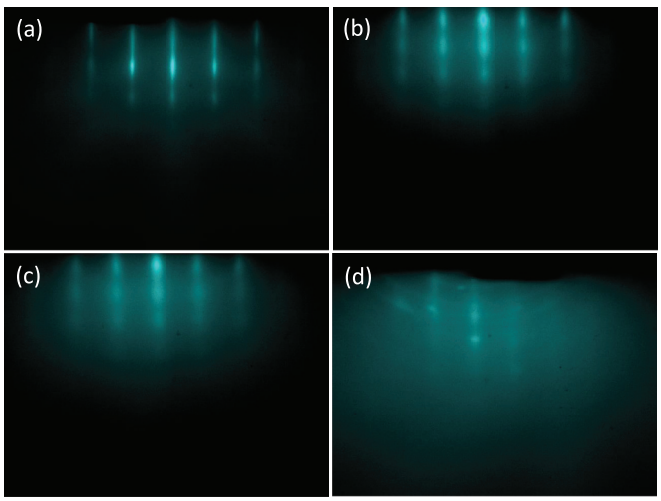

FIG. 1. (Color online) RHEED patterns taken along the [110] azimuth of Co-substituted $SrTiO_3$ for (a) 10%, (b) 30%, (c) 40%, and (d) 50% nominal cobalt composition. The diffraction patterns are taken using 18-keV electron energy at a grazing angle of 4°.

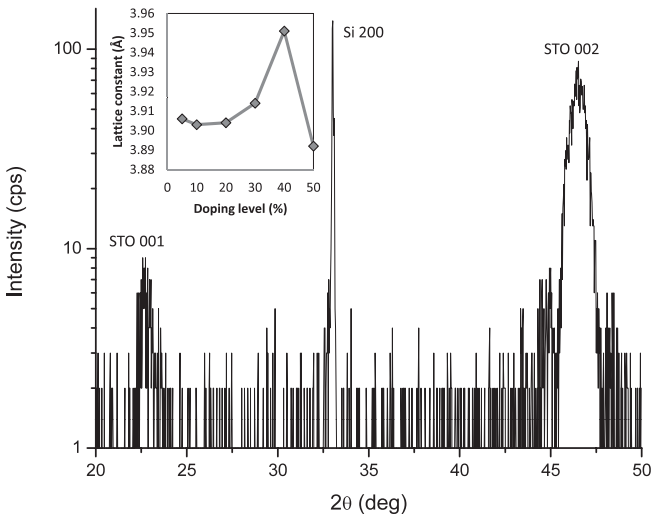

FIG. 2. X-ray diffraction 2θ-θ scan for 8-nm-thick 30% Co-substituted $SrTiO_3$. The only features observed are from the silicon substrate and from the $00l$ reflections of $SrTiO_3$. The inset on the upper left shows the c lattice constant as a function of nominal Co composition obtained from the 002 film Bragg reflection.

The RHEED pattern for 10% cobalt substitution [Fig. 1(a)] shows very sharp streaks similar to that obtained for undoped $SrTiO_3$ on Si. When the amount of cobalt is increased to 20–30% [Fig. 1(b)], the streaks become broader, indicative of a greater degree of crystalline disorder but still well defined and single phase. For 40% Co substitution [Fig. 1(c)], RHEED shows the appearance of weak extra spots that indicate the presence of incommensurate secondary phases. The appearance of secondary phases becomes even clearer at 50% cobalt composition, where polycrystalline arcs begin to emerge [Fig. 1(d)].

The cobalt-substituted films were measured using x-ray diffraction to determine lattice constants and bulk crystalline quality. For compositions of 10–40%, the symmetric 2θ-θ scan (Fig. 2) shows only peaks from the silicon substrate and the $00l$ crystal planes of $SrTiO_3$. The c axis lattice constant determined from the position of the 002 Bragg peak is shown in the inset in the upper left of Fig. 2. A small extra peak at $\sim 42^\circ$ is observed for 50% cobalt composition, which is attributed to CoO precipitates. A rocking curve measurement about the (002) $SrTiO_3$ peak for 10% cobalt yields a full width at half maximum of 0.4°, while a value of 0.7° is obtained for 30% cobalt.

Figure 3 is a cross-sectional high-resolution electron micrograph of a 5-nm 30% cobalt-substituted film grown on 1.5-nm undoped $SrTiO_3$/Si. The uniformity of the cobalt-substituted layer in Fig. 3 is evident. A wider area low-resolution scan of the same sample does not show the presence of precipitates. Figure 3 also shows that the initial undoped $SrTiO_3$ layer appears to have become amorphized and that a thin ($\sim$1.5 nm) SiO_x layer has also formed. The reason for the loss of crystallinity in the undoped $SrTiO_3$ layer are still unclear and may be due to either preferential amorphization as a result of the transmission electron microscopy (TEM) sample preparation[40] or to reaction of the thin $SrTiO_3$ layer with silicon-forming silicates and silicides.[41,42]

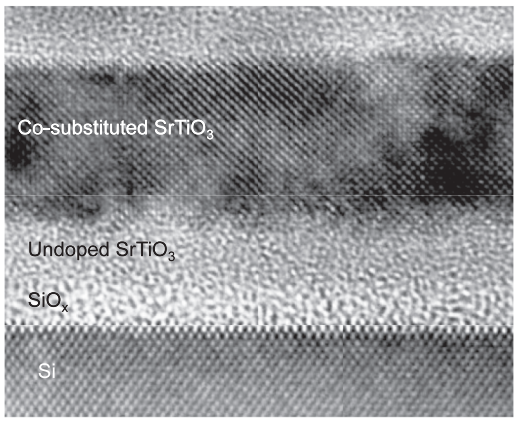

FIG. 3. High-resolution cross-section TEM images for 30% Co-substituted $SrTiO_3$ grown on four unit cells undoped $SrTiO_3$/Si. The uniform crystallinity of the Co-substituted layer is evident, but the image also shows amorphization of the undoped layer as well as a thin ($\sim$1.5 nm) SiO_2 layer.

B. X-ray photoelectron spectroscopy

The Co $2p$ spectrum (Fig. 4) shows a peak at 780.5 eV ($2p_{3/2}$) with a strong shake-up satellite feature at about 6-eV higher binding energy. This spectrum is consistent with previously reported spectra for Co in the +2 valence state[43,44] and confirmed by comparison to an epitaxial CoO thin film grown separately. There is no signal at 778 eV, confirming that there is no detectable free Co metal in the sample.[32] The Sr $3d$, Ti $2p$, and O $1s$ spectra (not shown) have qualitative features similar to *in situ* spectra for undoped $SrTiO_3$. The XPS high-resolution spectra for Sr $3d$, Ti $2p$, Co $2p$, and O $1s$ were also used to determine the stoichiometry of all films. Quantification was performed on 15-nm-thick films using Physical Electronics atomic sensitivity factors,[32]

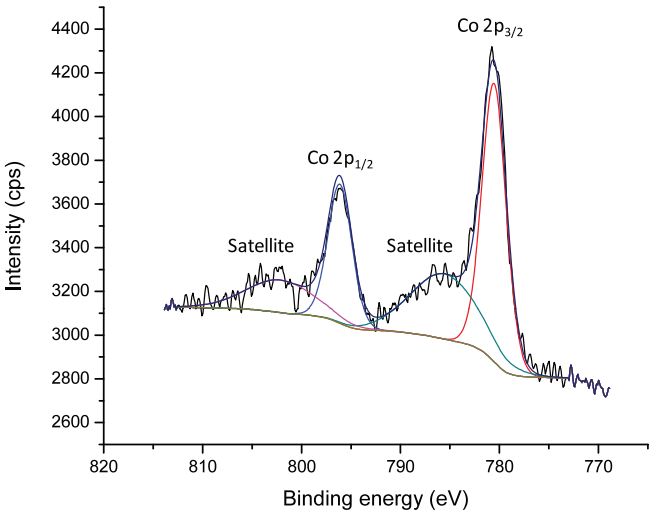

FIG. 4. (Color online) High-resolution x-ray photoelectron spectrum of the Co $2p$ core level in 30% Co-substituted $SrTiO_3$. The main $2p_{3/2}$ level is at 780.5 eV, with no feature associated with Co metal at 778 eV. Each spin-orbit split feature shows a strong shake-up satellite at about 6-eV higher binding energy, indicating that Co is primarily in the +2 valence state.

TABLE I. Composition of Co-substituted $SrTiO_3$ films for different nominal Co compositions as measured by high-resolution XPS. The integrated areas of the Sr *3d*, Ti *2p*, Co *2p*, and O *1s* spectra were used using appropriate sensitivity factors and corrected for sampling depth.

Nominal Co composition	Co/(Co + Ti)	Ti/(Co + Ti)	Sr/(Co + Ti)	O/(Co + Ti)
10%	0.12	0.88	1.06	2.90
20%	0.19	0.81	0.98	2.75
30%	0.32	0.68	0.95	2.65
40%	0.41	0.59	0.86	2.50
50%	0.42	0.58	0.80	2.45

corrected using a single-crystal $SrTiO_3$ standard. Integrated intensities of the entire spectrum including spin-orbit doublets are calculated using a Shirley background and corrected for using the analyzer transmission function. The kinetic energy dependence of the sampling depth is accounted for by using a kinetic energy exponent of 0.78, which was found to produce a Sr:Ti ratio of one for single-crystal $SrTiO_3$. Calculated stoichiometries for samples with various target cobalt compositions are given in Table I, which shows that the measured values for Co/(Co + Ti) are within ∼10% of the nominal cobalt composition. However, large Sr deficiencies are also observed for samples with 40–50% cobalt composition. Sr vacancies typically form in significant amounts only at temperatures higher than the growth temperature used in this study.[45] It appears that the presence of large amounts of Co in $SrTiO_3$ are promoting Sr vacancy formation, but further studies are needed to confirm this. Table I also shows the O/(Co + Ti) ratio for the different compositions. The amounts of oxygen in the films are all significantly less than the ideal ratio of three and correlate roughly with the amount of cobalt substitution plus amount of Sr deficiency. In particular, for 20% cobalt substitution, an oxygen ratio of 2.75 is observed, indicating as much as 25% oxygen deficiency in the film. This observation implies that cobalt substitution facilitates the removal of a nearly identical amount of oxygen (compensated doping). The effect of compensated cobalt-oxygen vacancy doping on the magnetic properties is detailed in Sec. IV F below.

C. Magnetic and transport properties

The magnetic properties of the cobalt-substituted films were measured using a Quantum Design superconducting quantum interference device (SQUID) magnetometer. The magnetization as a function of magnetic field was measured at 10 and 300 K. The field was applied in the plane of the film. The results of the 300-K measurement are shown in Fig. 5 for various cobalt compositions. The measurement shows paramagnetic behavior for low doping (10%). A small hysteresis opens up at 20% cobalt, and a well-defined hysteresis loop is observed at 30–40% cobalt. Based on the film volume used in the magnetic measurement, the saturation magnetic moment is calculated to be about 3.1 μ_B per Co with a remnant moment equivalent to 0.6 μ_B per Co. The 30% cobalt film also shows a coercive field of 95 Oe at room temperature, slightly larger than typical values reported for cobalt-doped anatase[17] and PLD-grown thin films of cobalt-doped $SrTiO_3$.[29] For very high cobalt concentrations (50%), magnetic ordering in the film is lost, and only diamagnetic behavior from the substrate is observed at room temperature. Measurement of magnetization vs temperature between 10 and 300 K shows no phase transition and only a gradual increase in the magnetic moment as temperature is decreased. This indicates that the Curie temperature of our films is above room temperature. It has been reported by Bi *et al.* that the Curie temperature for PLD-grown cobalt-substituted $SrTiO_3$ is higher than 1000 K.[29] Resistivity measurement of 20- to 40-nm ferromagnetic samples at room temperature shows a high sheet resistance of >1.1 GΩ/□, which is the resistance of the $SrTiO_3$ substrate. The measured sheet resistance increases rapidly as the temperature of the sample is decreased toward 77 K, quickly reaching the instrumental measurement limit. The high value of the sheet resistance and its increase upon cooling indicates that the Co-substituted $SrTiO_3$ is insulating.

D. Electronic structure of a single Co atom in $SrTiO_3$

In order to study the electronic structure and magnetic moment of an isolated Co atom, a dilute concentration of Co is needed. For this, we employ a $3 \times 3 \times 3$ supercell of $SrTiO_3$, where a single Ti atom is replaced by Co, resulting in a stoichiometry of $SrCo_xTi_{1-x}O_3$ with $x = 3.7\%$. Substituting a Ti atom in $SrTiO_3$ imparts a valency of +4 to Co meaning that it has five electrons to fill its valence states. Depending on the relative strength of the crystal-field splitting and Hund's coupling of the Co atom, these five electrons can either occupy only t_{2g} levels forming a low-spin $[(t_{2g}\uparrow)^3(t_{2g}\downarrow)^2]$ (1 μ_B) state, or occupy both e_g and t_{2g} levels forming a high-spin $[(t_{2g}\uparrow)^3(e_g\uparrow)^2]$ (5 μ_B) state. Our calculations indicate that Co stabilizes in the low spin state, where the majority of t_{2g} states are occupied, while one of the minority t_{2g} states is unoccupied. On the other hand, both the majority and minority spins of the e_g states are unoccupied. We also find that the influence of Co on Ti is short ranged. At a site located two lattice constants away, the Ti local DOS is essentially identical to that of the bulk $SrTiO_3$. This implies that any Co-Co interaction mediated by conduction electrons is short ranged.

E. Magnetic interaction between two neighboring Co atoms

To study the magnetic coupling between Co atoms, we now substitute two Ti atoms in the same supercell (the cell is sufficiently large to treat up to third-nearest neighbors) of $SrTiO_3$ with Co. We calculate the magnetic interaction for both first-nearest-neighbor Co atoms as well as second-nearest neighbors. For each case, we compare the total energy of a ferromagnetic ($E_{\uparrow\uparrow}$) and an antiferromagnetic ($E_{\uparrow\downarrow}$) configuration. Our calculations show that for nearest neighbor Co atoms, the ferromagnetic configuration is favored over the antiferromagnetic one by 60 meV/cell. However, when two Co atoms are arranged as second-nearest neighbors the ferromagnetic interaction becomes zero, confirming that the magnetic interaction between Co atoms in $SrTiO_3$ is short ranged. This suggests that, to induce ferromagnetism, Co atoms need to cluster close to each other. However,

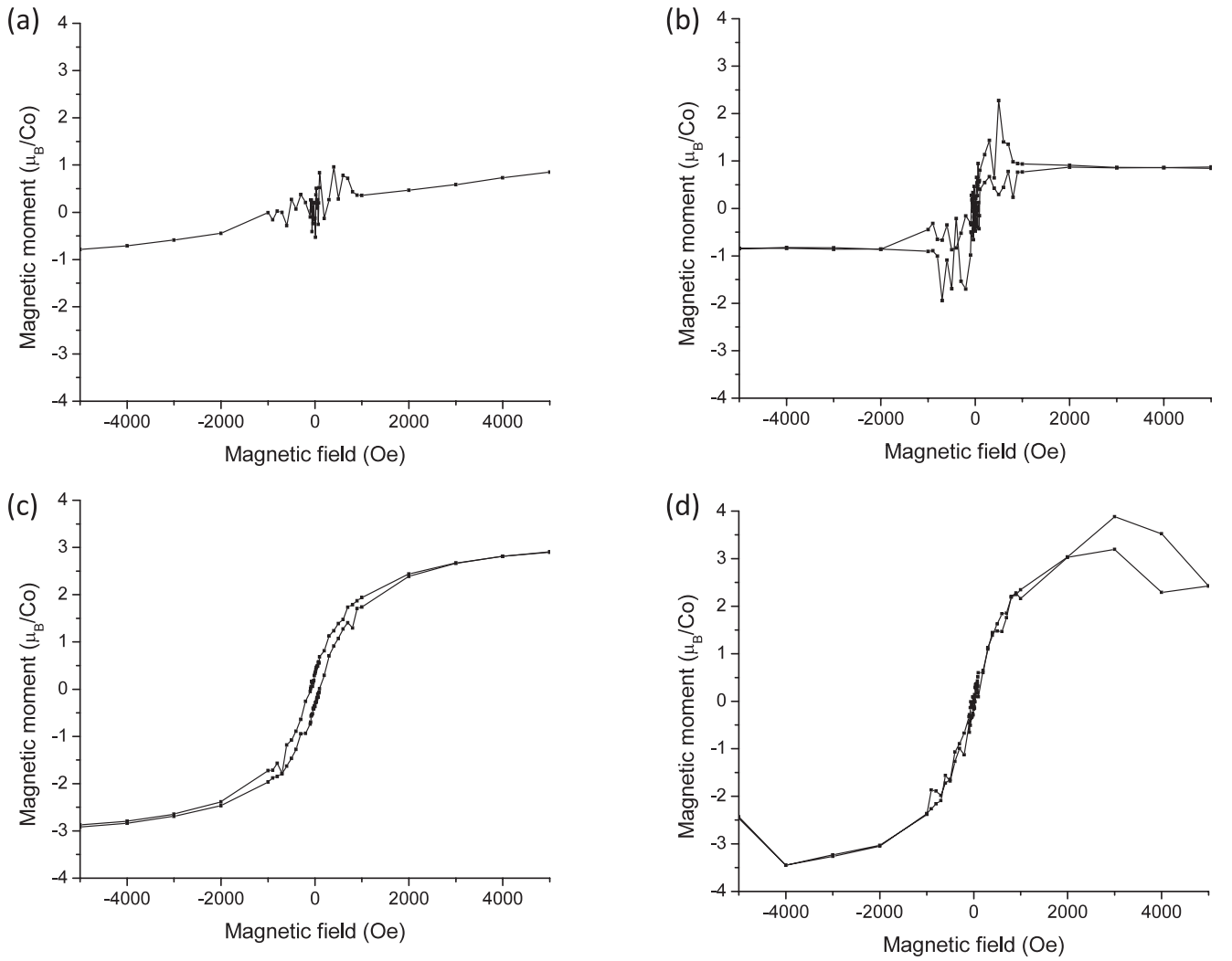

FIG. 5. Room-temperature magnetization vs magnetic field measurements for Co-substituted $SrTiO_3$ with different compositions: (a) 10%, (b) 20%, (c) 30%, and (d) 40% Co. The magnetic field is applied in the plane of the film and ranges from -5 to $+5$ kOe. At 10% Co, the film is paramagnetic. A small hysteresis loop opens up at 20%, becoming very well defined at 30–40%. The coercive field for 30% Co is 95 Oe with a saturation magnetic moment equivalent to $\sim 3.1\ \mu_B$/Co. At 50% Co (not shown), only a diamagnetic signal is observed.

comparing the total energy of the first- and second-nearest-neighbor configurations, we find that clustering of Co atoms is not energetically favored. Hence, extrinsic sources such as point defects are needed to stabilize the experimentally observed room-temperature ferromagnetism in Co-substituted $SrTiO_3$.

F. Role of oxygen vacancies

Because the presence of a significant number of oxygen vacancies in as-deposited MBE-grown Co-substituted $SrTiO_3$ is observed experimentally, they appear to be a likely source of enhancement of ferromagnetism in this system. While we also observe significant Sr vacancies at very large (40–50%) Co concentrations, because Sr vacancies in $SrTiO_3$ do not contribute to the formation of magnetic moments[46] and because they occur only when secondary phases begin to form, we will not consider them in the present theoretical analysis. The role of oxygen vacancies has been previously investigated by Griffin Roberts *et al.* for anatase[47] and by Florez *et al.* for $SrTiO_3$.[48] Griffin Roberts *et al.* show that in cobalt-doped anatase, a Co^{2+} interstitial coupled with Ti^{3+} via an oxygen vacancy are responsible for the observed ferromagnetism in cobalt-doped anatase with cobalt doping at the level of 3%.[47] In the study of Florez *et al.*, mixed spin states of Co^{3+}, in the presence of an oxygen vacancy, were found to produce ferromagnetic interactions between Co atoms in cobalt-doped $SrTiO_3$ at a doping level of 12.5%.[48] However, we find experimentally that robust magnetic ordering in cobalt-doped $SrTiO_3$ only occurs at higher concentrations of Co ($\sim$30%) and that Co is in the +2 valence state.

Theoretically, we model $SrTi_{1-x}Co_xO_{3-\delta}$ with a $2 \times 2 \times 2$ supercell to simulate the higher Co concentration. We first examine the effect of a single oxygen vacancy on a neighboring Co atom [Fig. 6(a)]. The first thing to check is whether vacancies are likely to occur in the vicinity of Co atoms. In order to do this, we compute the formation energy of an oxygen vacancy in the vicinity of a Co atom. This is done following the Zhang-

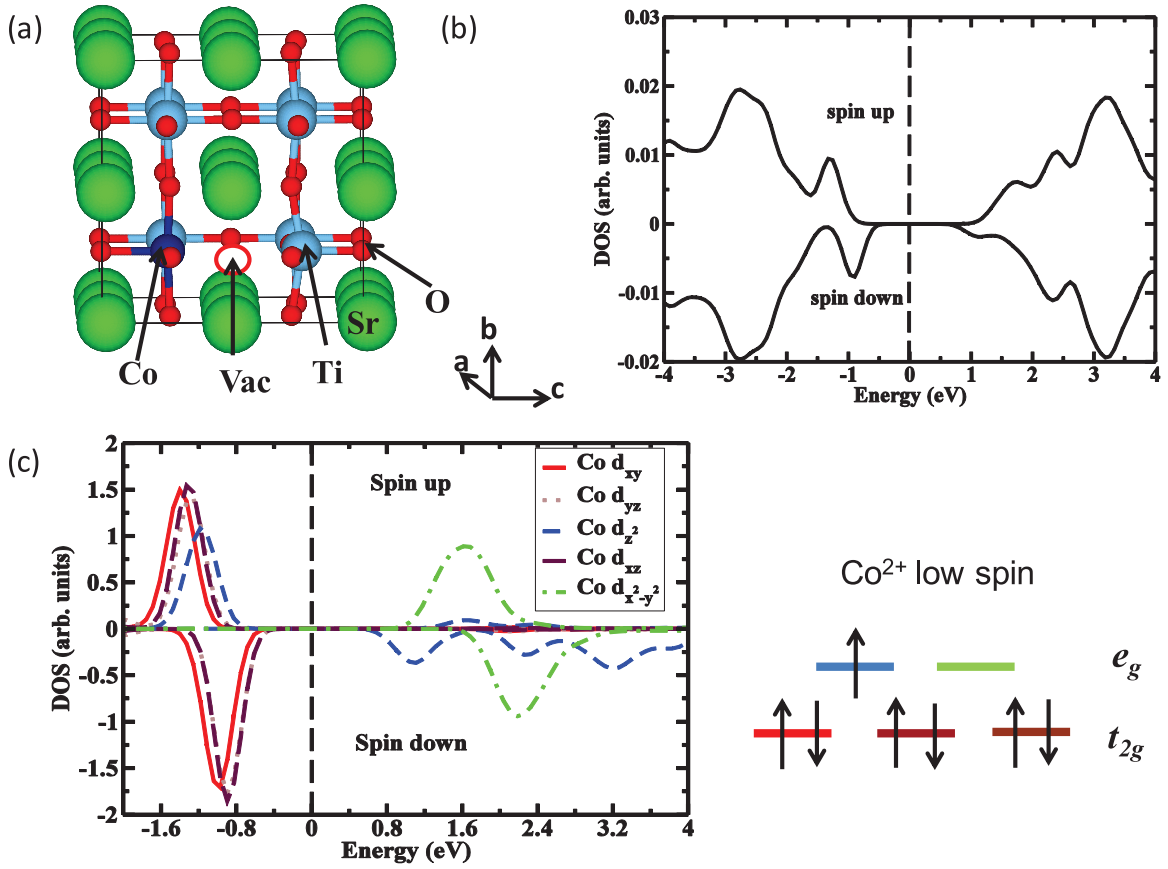

FIG. 6. (Color online) (a) Calculation supercell for one Co and one oxygen vacancy in $SrTiO_3$, with the oxygen vacancy next to the Co atom. The vacancy is directly on the right of Co (dark blue) in the figure. (b) Total DOS plot showing the existence of an energy gap resulting in insulating behavior. (c) Calculated local DOS for Co with an oxygen vacancy next to it for spin up (upper half) and spin down (lower half) electrons. The calculations indicate that Co is in the low spin Co^{2+} configuration

Northrup formalism.[49] The formation energy is given by

$$E_{\text{form}} = E_{\text{total}}(SrTi_{1-x}Co_xO_{3-\delta}) - E_{\text{total}}(SrTi_{1-x}Co_xO_3) - \mu_{O_2}, \quad (1)$$

where the first two terms are the total energies with and without an oxygen vacancy, respectively, and the last term is the chemical potential of oxygen taken as half of the binding energy of an oxygen molecule.[50] The formation energy of an oxygen vacancy in $SrTi_{1-x}Co_xO_{3-\delta}$ comes out to be 4.56 eV when it is placed adjacent to a Co atom at a distance of 1.93 Å. However, when the vacancy is placed 7 Å away from the Co atom, the formation energy increases to 5.84 eV. Hence, it is clear that oxygen vacancies are likely to occur near Co atoms. Compared to the neutral vacancy formation energy in undoped $SrTiO_3$, which is about 6.5eV,[51] the presence of a Co atom substantially (~2 eV) lowers the formation energy, because Co provides empty low-energy states for the two extra electrons associated with the vacancy to occupy. From this point on, we assume that the vacancy is adjacent to substitutional Co.

Before examining the electronic structure, it is interesting to point out the structural changes brought by the introduction of a Co-oxygen vacancy complex. The equilibrium lattice constant of bulk $SrTiO_3$ is found to be 3.92 Å within a local density approximation + U calculation. This means there is an overestimation of 0.5% compared to the experimental value of 3.90 Å. Upon the introduction of a Co-oxygen vacancy complex, we find that the equilibrium lattice constant of $SrTi_{1-x}Co_xO_{3-\delta}$ ($x = \delta = 0.125$) is reduced to 3.90 Å. As can be seen from the total DOS plot [Fig. 6(b)], the system is an insulator. An oxygen vacancy is an n-type defect and results in the donation of two electrons to the neighboring Co atom. This changes the cobalt valence state from Co^{4+} to Co^{2+}. With seven electrons in its outermost valence shell, we find that Co stabilizes in the low spin state with a magnetic moment of 1 μ_B. The orbitally resolved DOS plot of Co (in the presence of an oxygen vacancy) shows that while all its t_{2g} orbitals are completely filled, one of its e_g orbitals, the d_{z^2} orbital is half filled and the other, the $d_{x^2-y^2}$ is completely empty [Fig. 6(c)]. This results in stabilization of the low spin state.

Experimentally, a well-defined hysteresis loop and high-spin state are observed at a Co concentration of more than 20%. We therefore, now increase the concentration of Co to 25% with two Ti atoms being substituted by Co in the $2 \times 2 \times 2$ supercell. The occurrence of Co in the +2 valence state suggests that for every Co atom introduced, one needs a compensating oxygen vacancy. At this concentration, various configurations of Co and oxygen vacancies are possible. As

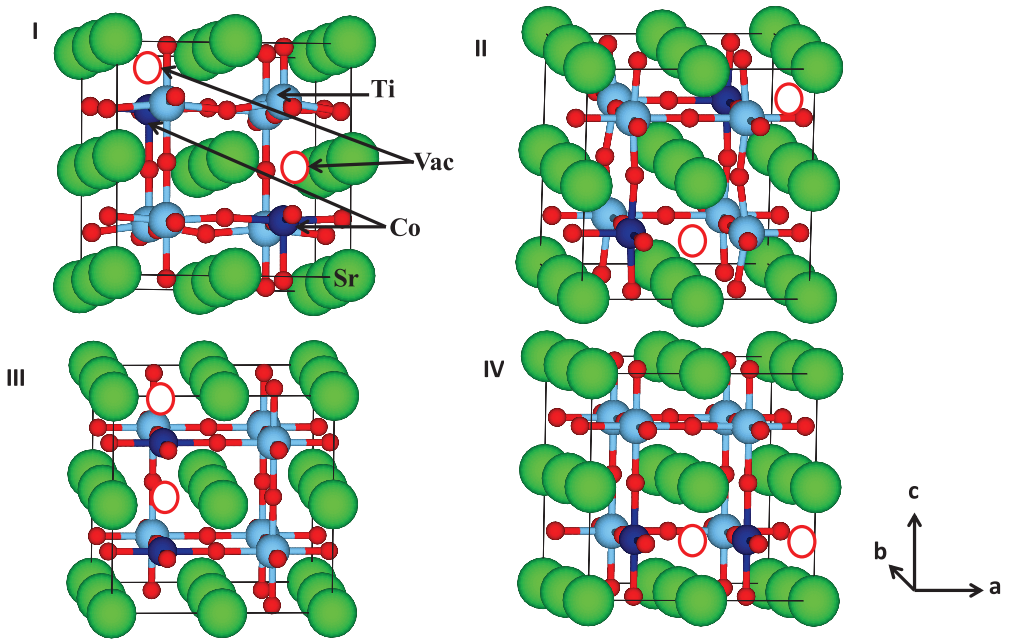

FIG. 7. (Color online) Four lowest-energy configurations for two Co atoms with adjacent oxygen vacancies in a 2 × 2 × 2 supercell.

we have shown earlier, oxygen vacancies are more likely to be found near a Co atom.

From in-plane x-ray diffraction measurements, the 20% Co-substituted $SrTiO_3$ sample on Si is under an in-plane tensile strain (1%), and an overall tetragonal distortion is present with the ratio between the out-of plane and in-plane lattice constants c/a being 0.989. We theoretically model this by fixing the in-plane lattice constant to 3.963 Å, which implies a 1% tensile strain in a theoretical structure, and then optimizing the out-of plane lattice constant c. There are many configurations possible for the Co atoms and vacancies at this concentration. In Fig. 7, we show the four lowest-energy structures. In structures I and II, Co atoms are placed along the body diagonal with vacancies along the c axis in I and along the a axis in II. In structures III and IV, the cobalt-vacancy complexes are aligned along the c and a axes, respectively. After relaxation, the resulting c/a ratios were found to be 0.973, 0.974, 0.969, and 0.975, respectively, for structures I, II, III and IV. Configuration IV is found to have the lowest energy, with the difference between E_{III} and E_{IV} being 164 meV/Co. Structures I and II are 359 and 320 meV/Co, respectively, higher in energy than structure IV. The in-plane tensile strain appears to stabilize a linear arrangement of Co-vacancy complexes along one of the in-plane directions. Structure IV is also found to be insulating in agreement with experiment. The calculated band gap for structure IV is 1.5 eV. An orbitally resolved local DOS (Fig. 8) of one of the Co atoms in structure IV shows one of the e_g orbitals and two of the t_{2g} orbitals to be half filled, indicating that Co is in the high-spin state with a magnetic moment of 3 μ_{B}/Co. The stabilization of one of the e_g states

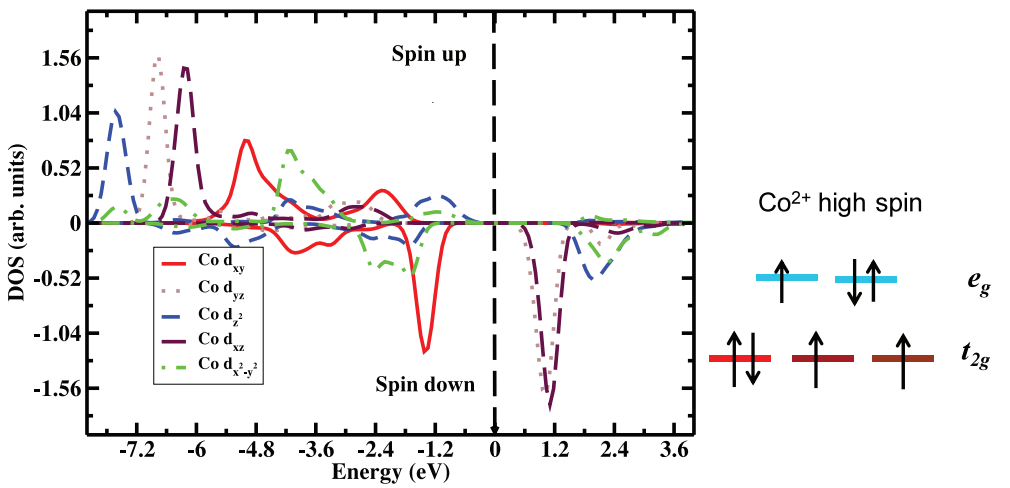

FIG. 8. (Color online) Local DOS for Co for the lowest energy configuration of two Co atoms plus two oxygen vacancies (configuration IV in Fig. 7). The Co stabilizes in the high spin state with a magnetic moment of 3 μ_{B}/Co.

(a combination of $d_{x^2-y^2}$ and d_{z^2} orbitals) originates from its local hybridization with the Co *4s* state in the presence of an oxygen vacancy.[52]

To summarize, our theoretical investigations imply that a combination of an oxygen vacancy and strain are crucial in order to explain our experimental observations. First, a Co ion and oxygen vacancy tend to form a complex and the two electrons provided by a vacancy are trapped at a Co site, consistent with the observed Co^{2+} state. The presence of Co lowers the formation energy of an oxygen vacancy by as much as 2 eV, consistent with the observation of the presence of an approximately equal number of oxygen vacancies as the amount of cobalt substitution. Second, a high concentration of Co (∼25%) is needed to stabilize the high spin state, in agreement with the occurrence of ferromagnetism only at cobalt concentrations greater than 20%. Finally, strain appears to stabilize the in-plane orientation of Co-vacancy complexes that result in an insulating state as measured experimentally.

V. CONCLUSIONS

We have successfully grown cobalt-substituted $SrTiO_3$ on silicon using MBE. Films with 30–40% cobalt show room-temperature ferromagnetism with a saturation moment of ∼3 μ_B/Co. XPS indicates that Co is in the +2 valence state and that an approximately equal number of oxygen vacancies are created by the cobalt substitution. Resistivity measurements show that the combination of cobalt substitution and oxygen vacancy creation, result in an insulating material. First-principles calculations reveal that oxygen vacancies are crucial in stabilizing ferromagnetism in this system and that a cobalt-oxygen vacancy complex is responsible for the observed insulating and magnetic behavior. This work shows a possible route for epitaxially integrating a room-temperature ferromagnetic insulator on silicon for potential use in spin-filtering-type injection contacts in spin-FETs.

ACKNOWLEDGMENTS

This work is supported by the National Science Foundation under Grants No. DMR-0548182 and No. DMR-1006725, the U.S. Department of Energy (DOE) under Grant No. DE-SC0001878, and Texas Advanced Computing Center. We are grateful to John Markert for the use of the SQUID magnetometer.

*E-mail: demkov@physics.utexas.edu

[1] S. A. Wolf, D. D. Awschalom, R. A. Buhrman, J. M. Daughton, S. von Molnar, M. L. Roukes, A. Y. Chtchelkanova, and D. M. Treger, Science **294**, 1488 (2001).
[2] S. Datta and B. Das, Appl. Phys. Lett. **56**, 665 (1990).
[3] G. Schmidt, D. Ferrand, L. W. Molenkamp, A. T. Filip, and B. J. van Wees, Phys. Rev. B **62**, R4790 (2000).
[4] R. Klasges, C. Carbone, W. Eberhardt, C. Pampuch, O. Rader, T. Kachel, and W. Gudat, Phys. Rev. B **56**, 10801 (1997).
[5] S. P. Dash, S. Sharma, R. S. Patel, M. P. de Jong, and R. Jansen, Nature (London) **462**, 491 (2009).
[6] B. T. Jonker, G. Kioseoglou, A. T. Hanbicki, C. H. Li, and P. E. Thompson, Nat. Phys. **3**, 542 (2007).
[7] A. H. MacDonald, P. Schiffer, and N. Samarth, Nat. Mater. **4**, 195 (2005).
[8] Y. Matsumoto, M. Murakami, T. Shono, T. Hasegawa, T. Fukumura, M. Kawasaki, P. Ahmet, T. Chikyow, S. Koshihara, and H. Koinuma, Science **291**, 854 (2001).
[9] S. Chambers, Surf. Sci. Rep. **61**, 345 (2006).
[10] S. J. Pearton, W. H. Heo, M. Ivill, D. P. Norton, and T. Steiner, Semicond. Sci. Technol. **19**, R59 (2004).
[11] C. Song, K. W. Geng, F. Zeng, X. B. Wang, Y. X. Shen, F. Pan, Y. N. Xie, T. Liu, H. T. Zhou, and Z. Fan, Phys. Rev. B **73**, 024405 (2006).
[12] K. Ueda, H. Tabata, and T. Kawai, Appl. Phys. Lett. **79**, 988 (2001).
[13] H. S. Kim, L. Bi, G. F. Dionne, C. A. Ross, and H. J. Paik, Phys. Rev. B **77**, 214436 (2008).
[14] S. B. Ogale, R. J. Choudhary, J. P. Buban, S. E. Lofland, S. R. Shinde, S. N. Kale, V. N. Kulkarni, J. Higgins, C. Lanci, J. R. Simpson *et al.*, Phys. Rev. Lett. **91**, 077205 (2003).
[15] J. Philip, A. Punnoose, B. I. Kim, K. M. Reddy, S. Layne, J. O. Holmes, B. Satpati, P. R. Leclair, T. S. Santos, and J. Moodera, Nat. Mater. **5**, 298 (2006).
[16] Y. K. Yoo, Q. Xue, H.-C. Lee, S. Cheng, X.-D. Xiang, G. F. Dionne, S. Xu, J. He, Y. S. Chu, S. D. Preite *et al.*, Appl. Phys. Lett. **86**, 042506 (2005).
[17] K. A. Griffin, A. B. Pakhomov, C. M. Wang, S. M. Heald, and K. M. Krishnan, Phys. Rev. Lett. **94**, 157204 (2005).
[18] S. A. Chambers, C. M. Wang, S. Thevuthasan, T. Droubay, D. E. McCready, A. S. Lea, V. Shutthanandan, and C. F. Windisch, Jr., Thin Solid Films **418**, 197 (2002).
[19] J. M. D. Coey, Curr. Opin. Solid State Mater. Sci. **10**, 83 (2006).
[20] K. J. Hubbard and D. G. Schlom, J. Mater. Res. **11**, 2757 (1996).
[21] T. C. Kaspar, T. Droubay, C. M. Wang, S. M. Heald, A. S. Lea, and S. A. Chambers, J. Appl. Phys. **97**, 073511 (2005).
[22] R. A. McKee, F. J. Walker, and M. F. Chisholm, Phys. Rev. Lett. **81**, 3014 (1998).
[23] C. Pascanut, N. Dragoe, and P. Berthet, J. Magn. Magn. Mater. **305**, 6 (2006).
[24] C. Decorse-Pascanut, J. Berthon, L. Pinsard-Gaudart, N. Dragoe, and P. Berthet, J. Magn. Magn. Mater. **321** 3526 (2009).
[25] S. Malo and A. Maignan, Inorg. Chem. **43**, 8169 (2004).
[26] P. Galinetto, A. Casiraghi, M. C. Mozazti, C. B. Azzoni, D. Norton, L. A. Boatner, and V. Trepakov, Ferroelectrics **368**, 120 (2008).
[27] D. Yao, X. Zhou, and S. Ge, Appl. Surf. Sci. **257**, 9233 (2011).
[28] S. X. Zhang, S. B. Ogale, Darshan C. Kundaliya, L. F. Fu, N. D. Browning, S. Dhar, W. Ramadan, J. S. Higgins, R. L. Greene *et al.*, Appl. Phys. Lett. **89**, 012501 (2006).
[29] L. Bi, H.-S. Kim, G. F. Dionne, and C. A. Ross, New J. Phys. **12**, 043044 (2010).
[30] G. Herranz, M. Basletić, M. Bibes, R. Ranchal, A. Hamzić, H. Jaffrès, E. Tafra, K. Bouzehouane, E. Jacquet, J. P. Contour *et al.*, J. Magn. Magn. Mater. **310**, 2111 (2007).

[31]M. Choi, A. Posadas, R. Dargis, C.-K. Shih, A. A. Demkov, D. H. Triyoso, N. D. Theodore, C. Dubourdieu, J. Bruley, and J. Jordan-Sweet, J. Appl. Phys. **111**, 064112 (2012).
[32]J. F. Moulder, W. F. Stickle, P. E. Sobol, and K. D. Bomben, *Handbook of X-Ray Photoelectron Spectroscopy*, edited by J. Chastain and R. C. King, Jr. (Perkin-Elmer Corporation, Eden Prairie, MN, 1995), p. 253.
[33]G. Kresse and J. Furthmüller, Phys. Rev. B **54**, 11169 (1996).
[34]P. E. Blöchl, Phys. Rev. B **50**, 17953 (1994).
[35]H. J. Monkhorst and J. D. Pack, Phys. Rev. B **13**, 5188 (1976).
[36]S. L. Dudarev, G. A. Botton, S. Y. Savrasov, C. J. Humphreys, and A. P. Sutton, Phys. Rev. B **57**, 1505 (1998).
[37]A. Y.-C. Yu and W. E. Spicer, Phys. Rev. **167**, 674 (1968).
[38]Y. Long, Y. Kaneko, S. Ishiwata, Y. Taguchi, and Y. Tokura, J. Phys.: Condens. Matter **23**, 245601 (2011).
[39]K. van Benthem and C. Elsässer, J. Appl. Phys. **90**, 6156 (2011).
[40]E. Eberg, A. F. Monsen, T. Tybell, A. T. J. Van Helvoort, and R. Holmestad, J. Electron Microsc. **57**, 175 (2008).
[41]G. J. Yong, R. M. Kolagani, S. Adhikari, W. Vanderlinde, Y. Liang, K. Muramatsu, and S. Friedrich, J. Appl. Phys. **108**, 033502 (2010).
[42]J. Q. He, C. L. Jia, V. Vaithnayathan, D. G. Schlom, J. Schubert, A. Gerber, H. H. Kohlstedt, and R. H. Wang, J. Appl. Phys. **97**, 104921 (2005).
[43]N. S. McIntyre and M. G. Cook, Anal. Chem. **47**, 2208 (1975).
[44]T. J. Chuang, C. R. Brundle, and D. W. Rice, Surf. Sci. **59**, 413 (1976).
[45]N.-H. Chan, R. K. Sharma, and D. M. Smyth, J. Electrochem. Soc. **128**, 1762 (1981).
[46]I. R. Shein and A. L. Ivanovskii, Phys. Lett. A **371**, 155 (2007).
[47]K. Griffin Roberts, M. Varela, S. Rashkeev, S. T. Pantelides, S. J. Pennycook, and K. M. Krishnan, Phys. Rev. B **78**, 014409 (2008).
[48]J. M. Florez, S. P. Ong, M. C. Onbaşli, G. F. Dionne, P. Vargas, G. Ceder, and C. A. Ross, Appl. Phys. Lett. **100**, 252904 (2012).
[49]S. B. Zhang and J. E. Northrup, Phys. Rev. Lett. **67**, 2339 (1991).
[50]R. O. Jones and O. Gunnarsson, Rev. Mod. Phys. **61**, 689 (1989).
[51]C. Mitra, C. Lin, J. Robertson, and A. A. Demkov, Phys. Rev. B **86**, 155105 (2012).
[52]C. Lin, C. Mitra, and A. A. Demkov, Phys. Rev. B **86**, 161102(R) (2012).